Ligand-mediated origin of altermagnetic spin splitting

Luigi Camerano [1,2,*] Federico Bisti [1] and Gianni Profeta [1,2]
[1]*Department of Physical and Chemical Sciences, University of L'Aquila, Via Vetoio, 67100 L'Aquila, Italy*
[2]*CNR-SPIN L'Aquila, Via Vetoio, 67100 L'Aquila, Italy*

(Received 22 May 2026; revised 19 October 2026; accepted 20 October 2026; published 5 November 2026)

Altermagnets host spin-split electronic bands despite zero net magnetization, opening new routes for spintronics beyond conventional ferromagnets. Going beyond symmetry-based classifications, which specify allowed terms but not their hierarchy, here we use first-principles calculations and Wannier Hamiltonian engineering to uncover the microscopic bonding contributions of altermagnetic spin splitting in the *g*-wave altermagnet $Co_{1/4}NbSe_2$. We show that the splitting is captured by a short-range tight-binding model, establishing its local origin. By selectively controlling hopping channels, we demonstrate that the dominant contribution arises not from direct magnetic-ion hopping, but from ligand-mediated hybridization that transfers anisotropy to itinerant states. This identifies ligand-assisted coupling as a dominant mechanism driving altermagnetic spin splitting in intercalated metals, providing a microscopic bridge between minimal models and material-specific electronic structure calculations in altermagnets.

DOI: 10.1103/s83n-w474

I. INTRODUCTION

Altermagnetism has garnered intense interest as a new class of collinear magnets that combine zero net magnetization with momentum-dependent spin-split electronic bands [1–8]. Unlike conventional ferromagnets, they retain spin-polarized band structures through the interplay of crystal symmetry and magnetic order [5,9–11]. This unique feature makes them promising for spintronics, enabling spin functionality without stray fields or magnetic interference, with potential applications in spin-current generation, anomalous transport, and ultrafast memory and logic devices [12–16].

This growing interest has stimulated an extensive search for realistic altermagnetic materials, combining first-principles predictions with experimental characterization to identify robust platforms for spin-split electronic structure [17–20]. Candidate systems now span metals [21–25], semimetals [26,27], oxides [28–31], and layered compounds [32–36]. In parallel, minimal Hamiltonian approaches serve as an important theoretical framework, providing a symmetry-based conceptual foundation for understanding altermagnetism. In particular, tight-binding (TB) models on square, honeycomb, Lieb, and related lattices [32,37–46] have shown how compensated magnetic sublattices, orbital anisotropy, and crystal symmetry can generate momentum-dependent spin splitting in the absence of both net magnetization and relativistic spin-orbit coupling. Together, these studies have opened the way to a classification of altermagnetic states in terms of ferroically ordered magnetic octupoles [47,48] and symmetry-harmonic decompositions of the spin density [49], while identifying characteristic transport responses and providing a unified framework for momentum-dependent spin textures. However, most existing models rely on hopping parameters chosen to satisfy symmetry constraints to capture the existence of altermagnetism, without identifying its microscopic origin in real compounds. In particular, the specific real-space electronic hopping processes, orbital pathways, and chemical bonds determining the altermagnetic spin splitting in real materials remain largely overlooked. In this paper, we propose a computational framework to uncover the chemical origin of altermagnetism through a real-space decomposition of hopping processes, enabled by first-principles Wannier Hamiltonian engineering. Similar Wannier-based hopping engineering approaches have recently been used to analyze magnetic exchange interactions in insulating two-dimensional (2D) magnets [50]. Here we extend this real-space framework to metallic altermagnets to isolate how momentum-dependent spin splitting is transferred to itinerant host states. As a representative case, we focus on an intercalated transition-metal dichalcogenide (TMD) $Co_{1/4}NbSe_2$, a system in which chemical composition and symmetry, and consequently the altermagnetic splitting, can be effectively tuned via straightforward processes such as intercalation.

Intercalated layered TMDs with transition-metal atoms such as Fe, Ni, Co, and Mn provide a particularly clean platform to address this problem. Indeed, in the TMD family, strong in-plane itinerancy coexists with strong sensitivity of the electronic and magnetic structure to interlayer stacking symmetry [24,51–53], resulting in a variety of electronic and magnetic phases. For example, in the 2H polytype, the interlayer symmetry combined with the A-type antiferromagnetic order of the intercalants, i.e., ferromagnetic layers stacked antiferromagnetically, enforces *g*-wave altermagnetic spin splitting as demonstrated by recent neutron diffraction [54],

*Contact author: luigi_camerano@outlook.it

Published by the American Physical Society under the terms of the Creative Commons Attribution 4.0 International license. Further distribution of this work must maintain attribution to the author(s) and the published article's title, journal citation, and DOI.

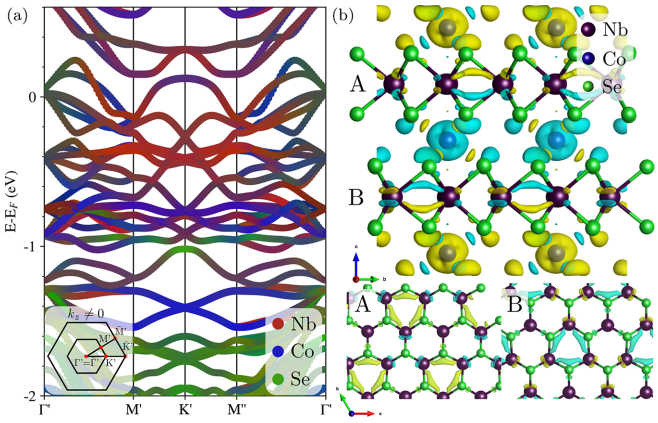


FIG. 1. (a) Atom-resolved projected band structure of $Co_{1/4}NbSe_2$ along high-symmetry lines for $k_z \neq 0$ from DFT calculations. The top-left inset shows the Brillouin zone (BZ) of the system: primed labels denote points at $k_z \neq 0$, while barred labels refer to the $NbSe_2$ BZ. (b) Top panel: magnetization-density isosurfaces with the b axis aligned along the x direction. The labels A and B identify the two inequivalent 2H-$NbSe_2$ layers in the unit cell. Bottom panel: top views of layers A and B, highlighting the induced magnetization on the Nb atoms.

muon spin rotation [55], and angle-resolved photoemission spectroscopy (ARPES) [23–25,56]. This realizes a layered altermagnetic state in which the altermagnetic symmetry originates from localized moments of the intercalant combined with the symmetry of the host TMD, resulting in the altermagnetic splitting of low-energy TMD derived bands. These systems thus provide direct access to the real-space mechanisms that transfer symmetry-driven spin splitting from the intercalant atom to the TMD layer. In particular, they enable the disentanglement of distinct hopping pathways, including direct magnetic–magnetic, ligand-assisted, and host-mediated contributions.

Taking $Co_{1/4}NbSe_2$ as a model system, we use first-principles calculations and Wannier-based Hamiltonians to identify the hopping channels responsible for transferring altermagnetic spin splitting to itinerant states, thereby providing a real-space framework to analyze the microscopic origin of spin splitting in intercalated metallic TMDs.

II. FIRST-PRINCIPLES ELECTRONIC STRUCTURE

We start by analyzing the electronic and magnetic structure of $Co_{1/4}NbSe_2$ using first-principles density functional theory (DFT) calculations (see Methods in the Appendix). Since our focus is on the nonrelativistic altermagnetic spin splitting experimentally observed in $Co_{1/4}NbSe_2$ and related intercalated TMDs [23–25,56], all DFT and Wannier-based tight-binding calculations are performed without spin-orbit coupling, thereby isolating the spin splitting arising from exchange interactions and crystal symmetry. As shown in Fig. 1(a), the bands crossing the Fermi level are predominantly Nb-derived, demonstrating that the low-energy sector is largely itinerant and hosted by the $NbSe_2$ layers. By contrast, Co states are concentrated at higher binding energy around ~ -1 eV, while the Se p manifold lies deeper near ~ -1.5 eV. This separation of energy scales naturally distinguishes localized magnetic degrees of freedom from itinerant carriers.The corresponding magnetization density [Fig. 1(b)] reveals pronounced local moments on Co together with a finite induced polarization on the otherwise nonmagnetic Nb atoms. Importantly, the sign and magnitude of the induced Nb magnetization depend on the inequivalent $NbSe_2$ layers, reflecting the layered A-type antiferromagnetic phase of the intercalants combined with the symmetry of the 2H phase. The Co magnetic moment is $\sim 1.4\,\mu_B$, resulting from the substantial screening by itinerant electrons, as observed in other intercalated compounds [53,57,58]. Thus, in $Co_{1/4}NbSe_2$, the altermagnetic spin polarization onto the metallic Nb bands originates from the peculiar coupling between localized Co-moments and itinerant host Nb bands.

III. LOCAL ORIGIN OF ALTERMAGNETIC SPIN SPLITTING

To uncover how this is microscopically realized,we construct a Wannier-based tight-binding Hamiltonian from the DFT electronic structure and use it to systematically control the real-space hopping processes in the system, selectively enabling individual hopping channels and orbital pathways. As long as this approach preserves the overall features of the DFT band structure, it enables a clear disentanglement of the microscopic contributions to the spin splitting. To guide the selection of physically relevant parameters, we first analyze the spatial range of the electronic processes by examining the hopping amplitudes as a function of interatomic distance [Fig. 2(a)], along with the corresponding histogram [Fig. 2(b)]. We then progressively truncate the Wannier Hamiltonian in real space using cutoff distances r_{c1} and r_{c2}, indicated in Figs. 2(a) and 2(b) in orange and green, respectively. The corresponding bonding networks are illustrated in Fig. 2(c), where green bonds denote r_{c2}, and both green and orange bonds represent r_{c1}. In Fig. 2(d), we present the Wannier interpolated bands from DFT calculations.

Retaining only the dominant short-range hoppings within $r_{c1} = 3.85$ Å [orange and green bonds in Fig. 2(c)] is already sufficient to reproduce the main band dispersions, along with the characteristic altermagnetic spin splitting of the full system [Fig. 2(d)]. This indicates that the essential mechanisms are predominantly local and do not rely on longer-range hopping processes. By contrast, further reducing the cutoff to $r_{c2} = 3.102$ Å, which eliminates the Nb–Nb and Se-Se hopping network [orange bonds in Fig. 2(c)], substantially modifies the spectrum, driving the system toward an insulating state with only a weak residual spin splitting. These results show that capturing the overall band structure of $Co_{1/4}NbSe_2$ requires the inclusion of the Nb–Nb and Se-Se network and hoppings [orange bonds in Fig. 2(c)], which sustain the dominant altermagnetic response. On the other hand, to clarify the microscopic origin of the spin anisotropy, we performed a symmetry analysis of the Co–Se sublattice. Remarkably, upon removing the Nb atoms while retaining the Co and Se atoms, the system preserves the same spin space group as the full structure, $P\bar{1}6_3/\bar{1}m1\bar{1}m1c^{\infty_{001}}m1$, which allows the observed g-wave spin splitting. This demonstrates that Nb is not required to establish the symmetry of the altermagnetic spin texture. Instead, the localized Co moments imprint

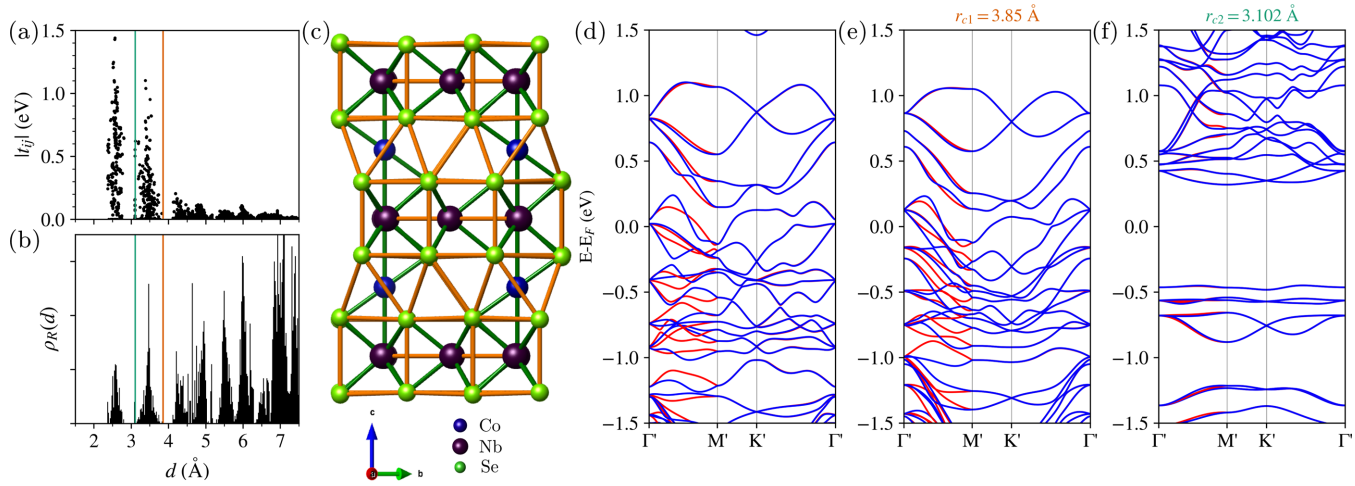


FIG. 2. (a) Absolute value of the hopping amplitudes as a function of interatomic distance. (b) Histogram of the hopping amplitudes at a given distance. The orange and green lines mark the cutoff radii used in panels (e) and (f) ($r_{c1} = 3.85$ Å and $r_{c2} = 3.102$ Å, respectively). (c) Unit cell of $Co_{1/4}NbSe_2$, where the bond colors indicate the hopping cutoff radius considered. (d) Wannier-interpolated band structure along high-symmetry lines, where blue and red denote spin-up and spin-down channels, respectively. Panels (e) and (f) show the band structures obtained by retaining only hoppings between atoms within cutoff distances $r_{c1} = 3.85$ Å and $r_{c2} = 3.102$ Å, respectively.

their nontrivial magnetic symmetry onto the surrounding Se ligands, as directly reflected by the opposite magnetization-density patterns around the spin-up and spin-down Co sites shown in Fig. 1(b). The Se-p orbitals, therefore, provide the symmetry-carrying channel through which the Co magnetic texture is transferred to the itinerant Nb-derived states via hybridization, giving rise to the observed g-wave spin splitting (see also the Supplemental Material [59] for band structure without hoppings to Nb ions).

IV. HOPPING-RESOLVED ANALYSIS OF THE SPIN SPLITTING

Motivated by the central role of the Nb and Se networks in determining the electronic structure, we take the $NbSe_2$-like electronic structure as a reference manifold and selectively restore individual couplings with the magnetic intercalants. This procedure allows us to isolate how distinct real-space pathways such as direct magnetic-ion hopping, ligand-assisted hybridization, and host-mediated processes contribute to the emergence of altermagnetic spin splitting. To this end, we decompose the truncated short-range Hamiltonian as

$$H^{(r_{c1})} = H_0 + \sum_{XY} H_{XY}. \tag{1}$$

Here H_0 is the Hamiltonian matrix containing the minimal hoppings terms which are needed to reproduce the $NbSe_2$ bands close to the Fermi level: hoppings between Nb-Se and Nb-Nb. H_{XY} is the part of the Hamiltonian matrix that includes the remaining interactions between Nb-Co, Co-Se, and Se-Se within the cutoff radius r_{c1}. Starting from the $NbSe_2$ host sector H_0, we then selectively activate individual couplings to determine their role in generating the altermagnetic band splitting [see Figs. 3(a)–3(d)]. In Fig. 3, we report the spin-resolved band structures along the high-symmetry lines of the 2H-$NbSe_2$ BZ at $k_z = 0.04\pi$ Å^{-1}, including different interactions (see below) together with its corresponding unfolding weights onto the primitive 2H-$NbSe_2$ unit cell (lower panels). Figures 3(a)–3(d) schematically indicate the $Co_{1/4}NbSe_2$ bonds retained in each calculation according to Eq. (1). Figure 3(a) shows the spectrum obtained from H_0 alone, where, as expected, no spin splitting is present. The flat bands present at –1 and 0 are the isolated on-site energies of the Co sublattices. Interestingly, we can demonstrate that these bands strongly resembles the DFT bands of the monolayer 1H-$NbSe_2$, after a rigid shift by 0.3 eV to account for charge transfer from the Co intercalants. We plot the DFT bands of the 1H phase (defined in the 1×1 primitive unit cell) in Fig. 3(l) (solid orange bands) compared with the corresponding TB bands (calculated in the 2×2 supercell) unfolded in the 1×1 unit cell (black lines, with line thickness proportional to the spectral weight). The differences between these two bands highlight the effect of the intercalant superperiodicity, which reconstructs the host electronic structure through gap openings at folded-band crossings. The strongest reconstruction occurs along $\bar{\Gamma}'\bar{K}'$, with smaller hybridization minigaps visible along $\bar{\Gamma}'\bar{M}'$ and $\bar{K}'\bar{M}'$.

We then selectively include H_{SeSe}, with the resulting spectrum shown in Fig. 3(f). The Se-Se hopping network restores the three-dimensional character of the electronic structure while preserving zero spin splitting, since couplings to the magnetic Co atoms are still absent. This is further illustrated in Fig. 3(m), where comparison with the DFT 2H-$NbSe_2$ bands shows that the splitting at $\bar{\Gamma}'$ and M′ originates from interlayer hybridization [32,60], while the locations of the gap openings remain essentially unchanged from the H_0 case. In addition, Se-derived down-dispersive bands emerge below -1 eV, consistent with the projected DFT spectrum of Fig. 1(a). The further inclusion of H_{NbCo}, shown in Figs. 3(g)–3(n), only weakly modifies the overall band structure but has a qualitative impact on the spin polarization. Remarkably, although H_{NbCo} does not itself contain anisotropic spin-dependent hoppings between antiferromagnetically ordered Co sites typically required to generate g-wave altermagnetism,

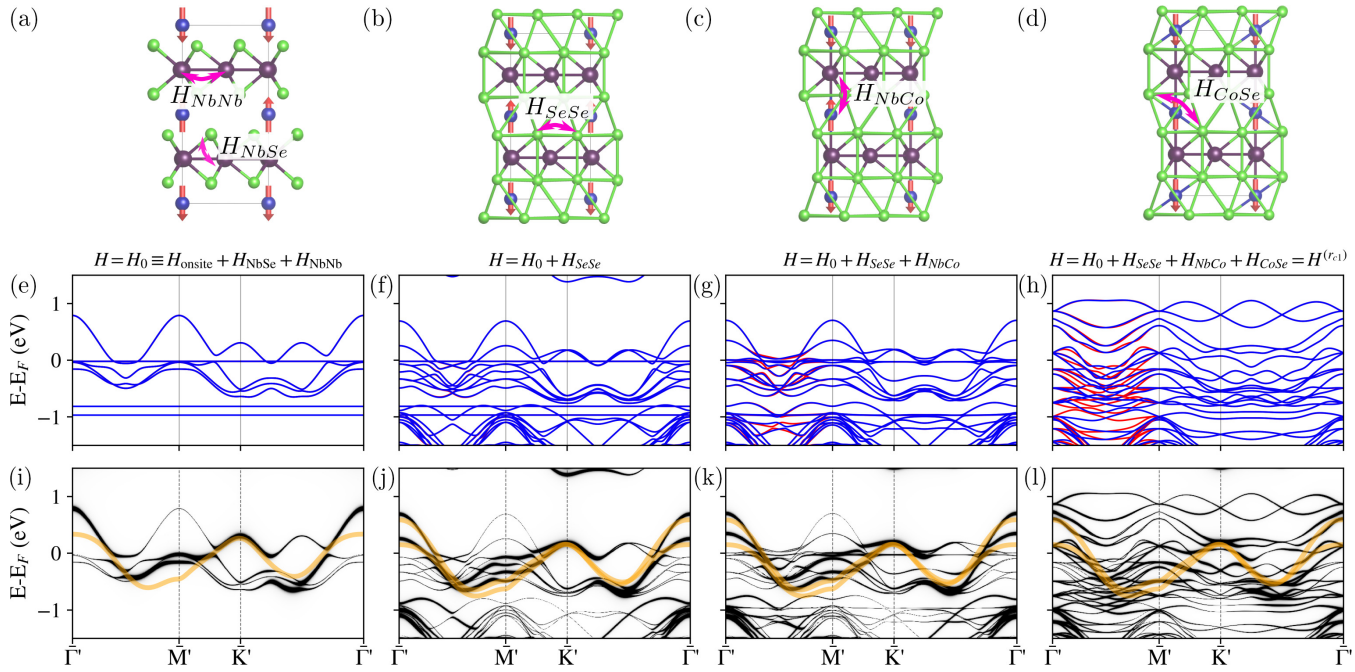


FIG. 3. (a)–(d) Unit cell, where only the retained hoppings are indicated as bonds. (e)–(h) Wannier-interpolated band structures obtained by selectively excluding specific hopping terms: (e) excluding Co–Se, Se–Se, and Co–Nb hoppings; (f) excluding Co–Se and Co–Nb hoppings; (g) excluding only Co–Se hoppings; and (h) including all hoppings within the cutoff radius $r_{c1} = 3.85$ Å. The insets show the unit cell, where only the retained hoppings are indicated as bonds. (i)–(l) Unfolded spectral weight projected onto the $NbSe_2$ unit cell for the same cases shown in panels (e)–(h). In panel (i), the solid orange lines correspond to the DFT band structure of a $NbSe_2$ monolayer. In panels (j)–(l), the solid orange lines represent the band structure of 2H-$NbSe_2$.

it nevertheless induces a finite spin splitting through its indirect coupling to the anisotropic Se network. In particular, despite the absence of direct anisotropic Nb-Co hopping, the Nb-derived bands near the Fermi level become strongly spin-polarized, demonstrating that the altermagnetic splitting is efficiently transferred to the itinerant states via ligand-mediated processes.

Indeed, as shown in the Supplemental Material [59], including H_{NbCo} while neglecting H_{SeSe} preserves the band degeneracy. This demonstrates that the spin splitting originates from an indirect ligand-mediated pathway involving the Se network. As seen in Fig. 3(n), the comparison with the 2H-$NbSe_2$ bands remains meaningful at this stage. In particular, the folded bands along $\bar{\Gamma}'\bar{K}'$ acquire finite spectral weight, partially filling the gap opened by the superperiodicity, while retaining the overall structure of the host-derived states. Finally, restoring H_{CoSe} completes the full Hamiltonian $H^{(r_{c1})}$ and fully recovers the g-wave altermagnetic spin splitting [see Fig. 3(h)]. In contrast to H_{NbCo}, this term directly introduces bond anisotropy tied to the Co sublattice, leading to a pronounced reconstruction of the electronic structure. As shown in Fig. 3(o), bands are strongly split and additional minigaps develop along $\bar{\Gamma}'\bar{K}'$, highlighting the central role of the intercalant in shaping the low-energy spectrum. The previously flat Co-derived states acquire a finite in-plane dispersion, signaling enhanced hybridization with the host. This analysis reveals a clear hierarchy of microscopic processes underlying altermagnetic spin splitting. While the $NbSe_2$ host sector sets the itinerant electronic structure and the Se network establishes the three-dimensional connectivity, neither is sufficient to generate spin splitting. The inclusion of H_{NbCo} introduces a finite but indirect contribution mediated by the ligand network, whereas the dominant mechanism arises from H_{CoSe}, which transfers the symmetry-breaking anisotropy of the Co sublattice to the itinerant Nb bands. These results identify ligand-assisted hybridization as the key channel through which altermagnetic spin splitting emerges in the metallic state.

V. TUNING LIGAND-MEDIATED SPIN SPLITTING

To quantify this mechanism, we continuously tune the Co–Se hybridization strength via a scaling dimensionless parameter λ, such that $H_{\text{CoSe}} \to \lambda H_{\text{CoSe}}$. Figure 4 shows the evolution of the band structure as a function of λ along the $\Gamma' M' \Gamma''$ high-symmetry line, with point size indicating the Nb orbital character. For $\lambda = 0$, the system exhibits weak spin splitting. Upon increasing λ, a momentum-dependent spin polarization develops in both Co- and Se-derived bands (one highlighted by thicker lines) and is subsequently transferred to Nb-derived states near the Fermi level. With increasing λ, initially flat Co-derived states approach the Nb bands and become progressively hybridized via the Se network. At large λ, the $NbSe_2$ band structure is strongly renormalized and the spin splitting at the Fermi level is reduced. In contrast, small deviations around $\lambda = 1$ have only a minor effect on the altermagnetic spin splitting, in agreement with the weak material dependence of the spin-splitting observed across

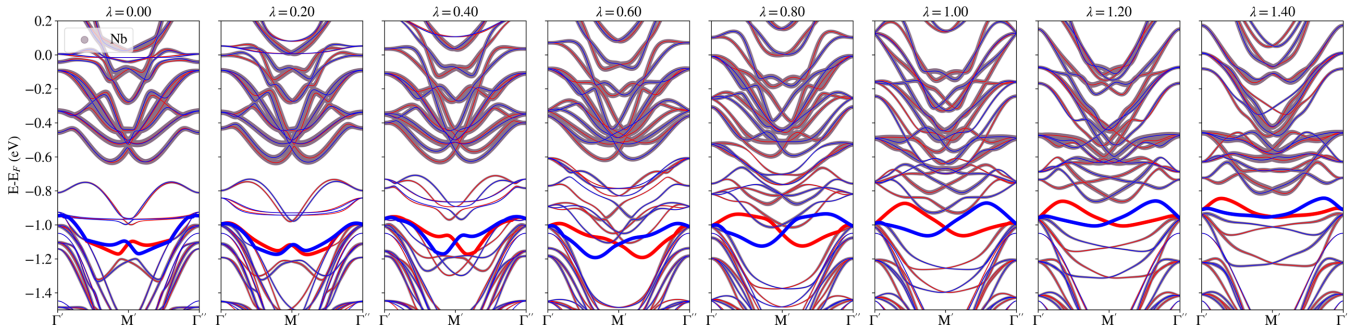


FIG. 4. Spin-resolved band structure as a function of the strength of the Co–Se hopping parameter $\lambda \in [0, 1.4]$. The size of the markers represents the projection weight on Nb atoms. The thicker bands highlight two representative states, chosen to track the evolution of the spin splitting.

different TMD hosts and intercalant species [61]. This weak sensitivity reflects that variations in material-specific parameters primarily renormalize microscopic Hamiltonian details without altering the overall scale of the induced spin splitting. This smooth evolution demonstrates that the altermagnetic spin splitting is continuously transmitted to the itinerant sector through ligand-mediated hybridization, providing direct microscopic evidence of its origin.

The intercalant-ligand bonding underlying this mechanism is experimentally accessible through core-level spectroscopy. In $Co_{1/4}NbSe_2$ and related intercalated TMDs, distinct ligand core-level components reveal the different electronic environments of surface ligands with reduced intercalant coordination and ligands retaining intercalant bonds [25,62]. These spectroscopic fingerprints support the importance of intercalant-ligand hybridization and motivate further investigation of how ligand coordination and bonding influence the spin splitting of itinerant states.

VI. CONCLUSIONS

In this work, we have identified the microscopic origin of altermagnetic spin splitting in $Co_{1/4}NbSe_2$ by combining first-principles calculations with a Wannier-based real-space decomposition of the electronic Hamiltonian. By selectively resolving and tuning individual hopping channels, we disentangled the different contribution to the altermagnetic spin splitting demonstrating that it is not rooted in direct magnetic-ion hopping, but is instead primarily generated through ligand-mediated Co–Se–Nb pathways. These processes transfer the symmetry of the magnetic sublattice to itinerant metallic states, establishing a direct real-space mechanism for altermagnetic band splitting in metallic systems. By connecting symmetry-based tight-binding descriptions with material-specific modeling, this work offers a clear real-space picture of how ligand hybridization shapes spin splitting in intercalated layered conductors, highlighting the importance of ligand physics.

ACKNOWLEDGMENTS

F.B. acknowledges funding from the National Recovery and Resilience Plan (NRRP), Mission 4, Component 2, Investment 1.1, funded by the European Union (NextGenerationEU), for the project "TOTEM" (CUP E53D23001710006 - Call for tender No. 104 published on 2/2/2022 and Grant Assignment Decree No. 957 adopted on 30/06/2023 by the Italian Ministry of Ministry of University and Research (MUR)) and for the project "SHEEP" (CUP E53D23018380001 - Call for tender No. 1409 published on 14/9/2022 and Grant Assignment Decree No. 1381 adopted on 01/09/2023 by the Italian Ministry of Ministry of University and Research (MUR)).

DATA AVAILABILITY

All data that support the findings of this study are included within the article and Supplemental Material [59].

APPENDIX: COMPUTATIONAL METHODS

Density functional theory calculations were performed using the Vienna *ab-initio* Simulation Package (VASP) [63,64], using the generalized gradient approximation (GGA) in the Perdew-Burke-Ernzerhof (PBE) parametrization for the exchange-correlation functional [65]. Interactions between electrons and nuclei were described using the projector-augmented wave method. Energy thresholds for the self-consistent calculation was set to 10^{-6} eV and force threshold for geometry optimization 10^{-4} eV Å^{-1}. A plane-wave kinetic energy cutoff of 550 eV was employed. The Brillouin zone was sampled using an $6 \times 6 \times 4$ Gamma-centered Monkhorst-Pack grid. We used experimental lattice parameters $a = 6.9178$ Å and $c = 12.390$ Å as determined by neutron diffraction [54]. All calculations were performed without an additional Hubbard U correction. This choice is motivated by recent ARPES studies showing good agreement between the measured electronic structure, including the low-energy band dispersions and altermagnetic spin splitting, and calculations performed without a Hubbard correction [25].

Maximally localized Wannier functions [66–68] are obtained by using WANNIER90 code [69] using atomic projection on Co-d, Nb-d, and Se-p orbital. The real-space Hamiltonian obtained from DFT bands is analyzed using the open-source code PythTB [70].

[1] L. Šmejkal, R. González-Hernández, T. Jungwirth, and J. Sinova, Crystal time-reversal symmetry breaking and spontaneous Hall effect in collinear antiferromagnets, Sci. Adv. **6**, eaaz8809 (2020).

[2] L. Šmejkal, J. Sinova, and T. Jungwirth, Beyond conventional ferromagnetism and antiferromagnetism: A phase with nonrelativistic spin and crystal rotation symmetry, Phys. Rev. X **12**, 031042 (2022).

[3] L. Šmejkal, J. Sinova, and T. Jungwirth, Emerging research landscape of altermagnetism, Phys. Rev. X **12**, 040501 (2022).

[4] P. G. Radaelli, Tensorial approach to altermagnetism, Phys. Rev. B **110**, 214428 (2024).

[5] P. Liu, J. Li, J. Han, X. Wan, and Q. Liu, Spin-group symmetry in magnetic materials with negligible spin-orbit coupling, Phys. Rev. X **12**, 021016 (2022).

[6] C. Song, H. Bai, Z. Zhou, L. Han, H. Reichlova, J. H. Dil, J. Liu, X. Chen, and F. Pan, Altermagnets as a new class of functional materials, Nat. Rev. Mater. **10**, 473 (2025).

[7] H.-Y. Ma, M. Hu, N. Li, J. Liu, W. Yao, J.-F. Jia, and J. Liu, Multifunctional antiferromagnetic materials with giant piezomagnetism and noncollinear spin current, Nat. Commun. **12**, 2846 (2021).

[8] M. Hu, X. Cheng, Z. Huang, and J. Liu, Catalog of *c*-paired spin-momentum locking in antiferromagnetic systems, Phys. Rev. X **15**, 021083 (2025).

[9] X. Chen, J. Ren, Y. Zhu, Y. Yu, A. Zhang, P. Liu, J. Li, Y. Liu, C. Li, and Q. Liu, Enumeration and representation theory of spin space groups, Phys. Rev. X **14**, 031038 (2024).

[10] Y. Jiang, Z. Song, T. Zhu, Z. Fang, H. Weng, Z.-X. Liu, J. Yang, and C. Fang, Enumeration of spin-space groups: Toward a complete description of symmetries of magnetic orders, Phys. Rev. X **14**, 031039 (2024).

[11] S.-W. Cheong and F.-T. Huang, Altermagnetism with noncollinear spins, npj Quantum Mater. **9**, 13 (2024).

[12] R. González-Hernández, L. Šmejkal, K. Výborný, Y. Yahagi, J. Sinova, T. Jungwirth, and J. Železný, Efficient electrical spin splitter based on nonrelativistic collinear antiferromagnetism, Phys. Rev. Lett. **126**, 127701 (2021).

[13] D.-F. Shao, S.-H. Zhang, M. Li, C.-B. Eom, and E. Y. Tsymbal, Spin-neutral currents for spintronics, Nat. Commun. **12**, 7061 (2021).

[14] Y. Guo, X. Zhang, Z. Huang, J. Chen, Z. Luo, J. Zhang, J. Li, Z. Zhang, J. Zhao, X. Han, and H. Wu, Quantum materials for spintronic applications, npj Spintron. **2**, 36 (2024).

[15] Z. Guo, X. Wang, W. Wang, G. Zhang, X. Zhou, and Z. Cheng, Spin-polarized antiferromagnets for spintronics, Adv. Mater. **37**, 2505779 (2025).

[16] R. Zarzuela, R. Jaeschke-Ubiergo, O. Gomonay, L. Šmejkal, and J. Sinova, Transport theory and spin-transfer physics in *d*-wave altermagnets, Phys. Rev. B **111**, 064422 (2025).

[17] J. Krempaský, L. Šmejkal, S. W. D'Souza, M. Hajlaoui, G. Springholz, K. Uhlířová, F. Alarab, P. C. Constantinou, V. Strocov, D. Usanov, W. R. Pudelko, R. González-Hernández, A. Birk Hellenes, Z. Jansa, H. Reichlová, Z. Šobáň, R. D. Gonzalez Betancourt, P. Wadley, J. Sinova, D. Kriegner, *et al.*, Altermagnetic lifting of Kramers spin degeneracy, Nature (London) **626**, 517 (2024).

[18] T. Osumi, S. Souma, T. Aoyama, K. Yamauchi, A. Honma, K. Nakayama, T. Takahashi, K. Ohgushi, and T. Sato, Observation of a giant band splitting in altermagnetic MnTe, Phys. Rev. B **109**, 115102 (2024).

[19] Y.-P. Zhu, X. Chen, X.-R. Liu, Y. Liu, P. Liu, H. Zha, G. Qu, C. Hong, J. Li, Z. Jiang, X.-M. Ma, Y.-J. Hao, M.-Y. Zhu, W. Liu, M. Zeng, S. Jayaram, M. Lenger, J. Ding, S. Mo, K. Tanaka, *et al.*, Observation of plaid-like spin splitting in a noncoplanar antiferromagnet, Nature (London) **626**, 523 (2024).

[20] O. J. Amin, A. Dal Din, E. Golias, Y. Niu, A. Zakharov, S. C. Fromage, C. J. B. Fields, S. L. Heywood, R. B. Cousins, F. Maccherozzi, J. Krempaský, J. H. Dil, D. Kriegner, B. Kiraly, R. P. Campion, A. W. Rushforth, K. W. Edmonds, S. S. Dhesi, L. Šmejkal, T. Jungwirth, *et al.*, Nanoscale imaging and control of altermagnetism in MnTe, Nature (London) **636**, 348 (2024).

[21] B. Jiang, M. Hu, J. Bai, Z. Song, C. Mu, G. Qu, W. Li, W. Zhu, H. Pi, Z. Wei, Y.-J. Sun, Y. Huang, X. Zheng, Y. Peng, L. He, S. Li, J. Luo, Z. Li, G. Chen, H. Li, *et al.*, A metallic room-temperature d-wave altermagnet, Nat. Phys. **21**, 754 (2025).

[22] F. Zhang, X. Cheng, Z. Yin, C. Liu, L. Deng, Y. Qiao, Z. Shi, S. Zhang, J. Lin, Z. Liu, M. Ye, Y. Huang, X. Meng, C. Zhang, T. Okuda, K. Shimada, S. Cui, Y. Zhao, G.-H. Cao, S. Qiao, *et al.*, Crystal-symmetry-paired spin–valley locking in a layered room-temperature metallic altermagnet candidate, Nat. Phys. **21**, 760 (2025).

[23] A. P. Sakhya, M. I. Mondal, M. Sprague, R. B. Regmi, A. K. Kumay, H. Sheokand, I. I. Mazin, N. J. Ghimire, and M. Neupane, Electronic structure of a layered altermagnetic compound $CoNb_4Se_8$, arXiv:2503.16670.

[24] N. Dale, O. A. Ashour, M. Vila, R. B. Regmi, J. Fox, C. W. Johnson, E. S. Barnard, A. Fedorov, A. Stibor, N. J. Ghimire, and S. M. Griffin, Relativistic and nonrelativistic spin splitting above and below the Fermi level in a *g*-wave altermagnet, arXiv:2411.18761.

[25] A. De Vita, C. Bigi, D. Romanin, M. D. Watson, V. Polewczyk, M. Zonno, F. Bertran, M. B. Petersen, F. Motti, G. Vinai, M. Tuniz, F. Cilento, M. Cuoco, B. M. Andersen, A. Kreisel, L. J. D'Onofrio, O. J. Clark, M. T. Edmonds, C. Candelora, M. Xu, *et al.*, Robust spin splitting and fermiology in the layered altermagnet $CoNb_4Se_8$, Adv. Mater. e75367 (2026).

[26] X. Yang, Z. Q. Wang, and H. H. Fu, Anisotropic spin transport enhanced by zero-dimensional weyl nodes in altermagnetic weyl semimetals, Adv. Funct. Mater. **36**, 2502516 (2025).

[27] W. Lu, S. Feng, Y. Wang, D. Chen, Z. Lin, X. Liang, S. Liu, W. Feng, K. Yamagami, J. Liu, C. Felser, Q. Wu, and J. Ma, Signature of topological surface bands in altermagnetic Weyl semimetal CrSb, Nano Lett. **25**, 7343 (2025).

[28] M. Leiviskä, R. Firouzmandi, K.-H. Ahn, P. Kubaščik, Z. Soban, S. P. Bommanaboyena, C. Müller, D. Kriegner, S. Sailler, D. Reustlen, M. Lammel, K. K. Bestha, M. Hývl, L. Šmejkal, J. Železný, A. U. B. Wolter, M. Scheufele, J. Fischer, M. Opel, S. Geprägs, *et al.*, Spin Hall magnetoresistance at the altermagnetic insulator/Pt interface, Phys. Rev. Mater. **9**, 084403 (2025).

[29] Z. Cui, Z. Zhu, X. Duan, B. Hao, X. Chen, J. Zhang, and T. Zhou, Symmetry-driven unconventional magnetoelectric coupling in perovskite altermagnets: From bulk to the two-dimensional limit, Adv. Sci. e00004 (2026).

[30] T. Zhang, L. Yuan, J. M. Rondinelli, H. A. Fertig, and S. Zhang, Tunable hidden altermagnetic spin splitting in

layered ruddlesden–popper oxides, Nano Lett. **26**, 2778 (2026).
[31] S. Bandyopadhyay, S. Picozzi, and S. Bhowal, Designing nonrelativistic spin splitting in oxide perovskites, Phys. Rev. B **112**, 064405 (2025).
[32] L. Camerano, A. O. Fumega, J. L. Lado, A. Stroppa, and G. Profeta, Multiferroic nematic d-wave altermagnetism driven by orbital-order on the honeycomb lattice, npj 2D Mater. Appl. **9**, 75 (2025).
[33] C. Yu and J. L. Lado, Intrinsic *i*-wave altermagnetism in 2D graphene superlattices, Adv. Sci. e78167 (2026).
[34] Z. Zhu, X. Duan, J. Zhang, B. Hao, I. Žutić, and T. Zhou, Two-dimensional ferroelectric altermagnets: From model to material realization, Nano Lett. **25**, 9456 (2025).
[35] J. Sødequist and T. Olsen, Two-dimensional altermagnets from high throughput computational screening: Symmetry requirements, chiral magnons, and spin-orbit effects, Appl. Phys. Lett. **124**, 182409 (2024).
[36] Y. Liu, J. Yu, and C.-C. Liu, Twisted magnetic van der Waals bilayers: An ideal platform for altermagnetism, Phys. Rev. Lett. **133**, 206702 (2024).
[37] M. Roig, A. Kreisel, Y. Yu, B. M. Andersen, and D. F. Agterberg, Minimal models for altermagnetism, Phys. Rev. B **110**, 144412 (2024).
[38] R. González-Hernández and B. Uribe, Model Hamiltonian for altermagnetic topological insulators, Phys. Rev. B **112**, 184101 (2025).
[39] M. Dürrnagel, H. Hohmann, A. Maity, J. Seufert, M. Klett, L. Klebl, and R. Thomale, Altermagnetic phase transition in a Lieb metal, Phys. Rev. Lett. **135**, 036502 (2025).
[40] M. Dürrnagel, L. Klebl, T. Müller, R. Thomale, and M. Klett, Extended s-wave altermagnets arXiv:2508.20163.
[41] J. Issing, J. Seufert, M. Klett, S. Mazumdar, Y. Iqbal, R. Thomale, and A. Maity, Engineering altermagnetic orders on the square-kagome lattice through sublattice interference, Phys. Rev. B **114**, 115128 (2026).
[42] V. Leeb, A. Mook, L. Šmejkal, and J. Knolle, Spontaneous formation of altermagnetism from orbital ordering, Phys. Rev. Lett. **132**, 236701 (2024).
[43] P. Das, V. Leeb, J. Knolle, and M. Knap, Realizing altermagnetism in Fermi-Hubbard models with ultracold atoms, Phys. Rev. Lett. **132**, 263402 (2024).
[44] V. P. Kravchuk, K. V. Yershov, J. I. Facio, Y. Guo, O. Janson, O. Gomonay, J. Sinova, and J. van den Brink, Chiral magnetic excitations and domain textures of *g*-wave altermagnets, Phys. Rev. B **112**, 144421 (2025).
[45] N. Jana, A. Chakraborty, A. Mukherjee, and A. Agarwal, Layered topological antiferromagnetic metal at room temperature: $YbMn_2Ge_2$, Phys. Rev. B **112**, 075127 (2025).
[46] N. Jana, A. Chakraborty, A. Mukherjee, and A. Agarwal, Correlation-driven orbital order realizes 2D metallic altermagnetism, arXiv:2603.25426.
[47] S. Bhowal and N. A. Spaldin, Ferroically ordered magnetic octupoles in *d*-wave altermagnets, Phys. Rev. X **14**, 011019 (2024).
[48] S. Han, D. Jo, I. Baek, S. Cheon, P. M. Oppeneer, and H.-W. Lee, Harnessing magnetic octupole Hall effect to induce torque in altermagnets, Phys. Rev. Lett. **135**, 076705 (2025).
[49] R. Jaeschke-Ubiergo, V.-K. Bharadwaj, W. Campos, R. Zarzuela, N. Biniskos, R. M. Fernandes, T. Jungwirth, J. Sinova, and L. Šmejkal, Atomic altermagnetism, arXiv:2503.10797.
[50] D. Šabani, C. Bacaksiz, and M. V. Milošević, Beyond orbitally resolved magnetic exchange in CrI_3 and NiI_2, Phys. Rev. Lett. **135**, 036704 (2025).
[51] L. Camerano, D. Mastrippolito, D. Pierucci, J. Dai, M. Tallarida, L. Ottaviano, G. Profeta, and F. Bisti, Darkness in interlayer and charge density wave states of $2H$-TaS_2, Phys. Rev. B **111**, L121112 (2025).
[52] W. Li, J. T. Reichanadter, S. Wu, J. S. Oh, R. Basak, S. C. Haley, S. Wang, J. E. C. Mata, E. Vescovo, D. Lu, M. Hashimoto, C. Klewe, S. Sarker, J. L. McChesney, A. Frañó, J. G. Analytis, R. J. Birgeneau, J. B. Neaton, and Y. He, Electronic origin of delicate antiferromagnetism in Fe_xNbS_2, Phys. Rev. Lett. **136**, 216503 (2026).
[53] L. Camerano, E. A. Martínez, V. Porée, L. Martella, D. Mastrippolito, D. Pierucci, F. D'Orazio, P. M. Sheverdyaeva, P. Moras, E. Della Valle, T. Yu, M. Hoesch, C. M. Polley, T. Balasubramanian, A. Nicolaou, L. Ottaviano, V. N. Strocov, G. Profeta, and F. Bisti, Emergent 3D fermiology and magnetism in an intercalated van der Waals system, Adv. Sci. **13**, e76533 (2026).
[54] R. B. Regmi, H. Bhandari, B. Thapa, Y. Hao, N. Sharma, J. McKenzie, X. Chen, A. Nayak, M. El Gazzah, B. G. Márkus, L. Forró, X. Liu, H. Cao, J. F. Mitchell, I. I. Mazin, and N. J. Ghimire, Altermagnetism in the layered intercalated transition metal dichalcogenide $CoNb_4Se_8$, Nat. Commun. **16**, 4399 (2025).
[55] J. N. Graham, T. J. Hicken, R. B. Regmi, M. Janoschek, I. Mazin, H. Luetkens, N. J. Ghimire, and Z. Guguchia, Local probe evidence supporting altermagnetism in $Co_{1/4}NbSe_2$, Phys. Rev. Res. **8**, 023361 (2026).
[56] M. Sprague, M. I. Mondal, A. P. Sakhya, R. B. Regmi, S. Sadhukhan, A. K. Kumay, H. Sheokand, I. I. Mazin, N. J. Ghimire, and M. Neupane, Observation of altermagnetic spin splitting in an intercalated transition metal dichalcogenide Nat. Commun. **17**, 9935 (2025).
[57] P. Park, W. Cho, C. Kim, Y. An, Y.-G. Kang, M. Avdeev, R. Sibille, K. Iida, R. Kajimoto, K. H. Lee, W. Ju, E.-J. Cho, H.-J. Noh, M. J. Han, S.-S. Zhang, C. D. Batista, and J.-G. Park, Tetrahedral triple-Q magnetic ordering and large spontaneous Hall conductivity in the metallic triangular antiferromagnet $Co_1/3TaS_2$, Nat. Commun. **14**, 8346 (2023).
[58] H. Takagi, R. Takagi, S. Minami, T. Nomoto, K. Ohishi, M.-T. Suzuki, Y. Yanagi, M. Hirayama, N. D. Khanh, K. Karube, H. Saito, D. Hashizume, R. Kiyanagi, Y. Tokura, R. Arita, T. Nakajima, and S. Seki, Spontaneous topological Hall effect induced by non-coplanar antiferromagnetic order in intercalated van der Waals materials, Nat. Phys. **19**, 961 (2023).
[59] See Supplemental Material at http://link.aps.org/supplemental/10.1103/s83n-w474 for discussion of bands without Nb ions and role of Nb-Co hopping.
[60] F. Weber, R. Hott, R. Heid, L. L. Lev, M. Caputo, T. Schmitt, and V. N. Strocov, Three-dimensional Fermi surface of $2h-NbSe_2$: Implications for the mechanism of charge density waves, Phys. Rev. B **97**, 235122 (2018).
[61] E. Day-Roberts, H. Wu, O. Erten, and A. S. Botana, An altermagnetic materials library in intercalated transition-metal dichalcogenides, arXiv:2601.02481.

[62] L. Camerano, L. Martella, L. Battaglia, F. Giannessi, F. Camilli, L. Lozzi, P. M. Sheverdyaeva, P. Moras, L. Ottaviano, G. Profeta, and F. Bisti, Plasmon engineering in intercalated 2H-TaS_2, Nano Lett. **26**, 9083 (2026).

[63] G. Kresse and J. Hafner, *Ab initio* molecular dynamics for liquid metals, Phys. Rev. B **47**, 558 (1993).

[64] G. Kresse and D. Joubert, From ultrasoft pseudopotentials to the projector augmented-wave method, Phys. Rev. B **59**, 1758 (1999).

[65] J. P. Perdew, K. Burke, and M. Ernzerhof, Generalized gradient approximation made simple, Phys. Rev. Lett. **77**, 3865 (1996).

[66] N. Marzari and D. Vanderbilt, Maximally localized generalized Wannier functions for composite energy bands, Phys. Rev. B **56**, 12847 (1997).

[67] I. Souza, N. Marzari, and D. Vanderbilt, Maximally localized Wannier functions for entangled energy bands, Phys. Rev. B **65**, 035109 (2001).

[68] N. Marzari, A. A. Mostofi, J. R. Yates, I. Souza, and D. Vanderbilt, Maximally localized Wannier functions: Theory and applications, Rev. Mod. Phys. **84**, 1419 (2012).

[69] G. Pizzi, V. Vitale, R. Arita, S. Blügel, F. Freimuth, G. Géranton, M. Gibertini, D. Gresch, C. Johnson, T. Koretsune, J. Ibañez-Azpiroz, H. Lee, J.-M. Lihm, D. Marchand, A. Marrazzo, Y. Mokrousov, J. I. Mustafa, Y. Nohara, Y. Nomura, L. Paulatto, *et al.*, Wannier90 as a community code: New features and applications, J. Phys.: Condens. Matter **32**, 165902 (2020).

[70] T. Cole, S. Coh, and D. Vanderbilt, Python tight binding (PythTB) (Version 2.0.0) [Computer software] Zenodo, 2025, https://doi.org/10.5281/zenodo.17595433.